Comparative Study Of Back EMF Based Sensorless Control Methods For Dual Three-Phase PMSM

Linhui Fan, Tao Yang, Mohamed Rashed, Serhiy Bozhko
Department of Electrical and Electronics Engineering, University of Nottingham, Nottingham, UK
Email: Tao.Yang@nottingham.ac.uk

***Abstract*—Multiphase electrical machines have gained increased attentions recently due to its fault tolerance capability which is of great importance for more-electric aircraft application. This paper studies sensorless control of a high-speed dual three-phase electrical machine for turboprop aircraft green taxiing motor and engine generator applications. After introduction of a detailed mathematical model of a dual three-phase permanent magnet machine, two different types of back EMF based sensorless control are compared in this paper. The first method uses a phase-locked-loop (PLL) type speed and rotor position estimator and the other uses a Luenberger observer estimator. The effectiveness of these two different methods is demonstrated using simulations in the Matlab/Simulink environment. The comparison studies show that Luenberger type estimator has better dynamic performance but suffers high frequency noise in the estimated speed error and requires the use of machinal parameters. In contrast, PLL type estimator has inferior but acceptable performance. Its low-pass characteristics frees it from the high frequency noise. Moreover, it does not require the use of mechanical parameters.**

Keywords—Dual Three-Phase PMSM, Sensorless Control, Back EMF Sensorless Control Method.

I. INTRODUCTION

Over the last few decades, there has been tremendous progress in the efforts to move toward more electric aircraft (MEA). Many subsystems that previously used hydraulic, mechanical, and pneumatic power have been fully or partially replaced by electrical systems. Multiphase machine has been widely used in MEA [1] since it can provide notable improvements in various aspects of performance when compared with the use of conventional three-phase machine [2]. Multiphase machine exhibits outstanding advantages, such as reduced phase current rating as well as torque ripple, less DC link harmonic current; smooth magneto motive force (MMF), improved efficiency, and excellent fault tolerant characteristics [2-5]. In addition, the system reliability is greatly improved with multiphase machines since the machine can operate continuously even if one or several phases (in some cases) are lost [1]. One of the various multiphase drive solutions is the dual three-phase (DTP) machine that has two identical star-connected three-phase stator windings with isolated neutral points [6]. Considering the spatially shifted angle between two sets of three-phase windings, DTP machines can be classified as symmetrical (shifted by 60 electrical degrees) machines and asymmetric (shifted by 30 electrical degrees) machines. According to [7], symmetric DTP-PMSM is preferred to satisfy the severe fault-tolerant requirements that are imposed by the specific aerospace application. Hence, in this study, a symmetric DTP-PMSM is investigated to try to develop a mechatronic device for turboprop aircraft applications. The electrical machine is used for green taxiing application and driving propellers during motoring mode. During the generation mode, the electrical machine is driven by the engine and runs as an electrical generator. The schematic diagram of the machine is shown in Fig. 1.

Sensorless control is required in this study because the space in the gear-box is too small to install mechanical speed/position sensors. Besides, system reliability is improved since vulnerable components such as mechanical sensors in entire system are removed. Generally, sensorless control methods can be divided into two categories [8]. One is rotor saliency based methods such as high frequency signal injection approaches [9, 10]. The other one is a back EMF based method. In this study, the characteristics of the estimated back EMF signals are analyzed. The differences between a phase-locked-loop (PLL) type estimator and a Luenberger observer type speed and position estimator are compared. Sensorless control design for symmetric DTP-PMSMs has not been studied in details in existing publications and this paper undertakes the attempt to fill this gap.

II. DUAL THREE-PHASE PMSM MODEL

In this section, mathematic models of DTP-PMSM are built in three-phase coordinate frame, dq rotating frame and $\alpha\beta$ stationary frame.

A. Mathematical Model in Three-Phase Coordinate Frame

The voltage and flux equations of a DTP-PMSM in original phase coordinate frame can be written as

$$\boldsymbol{u_s} = R\boldsymbol{i_s} + \frac{d\boldsymbol{\varphi_s}}{dt} \tag{1}$$

$$\boldsymbol{\varphi_s} = \boldsymbol{L_s i_s} + \boldsymbol{\lambda}\varphi_m \tag{2}$$

where

$\boldsymbol{u_s} = [u_A \quad u_A \quad u_C \quad u_U \quad u_V \quad u_W]^T$ is a vector of stator voltages,

$\boldsymbol{i_s} = [i_A \quad i_B \quad i_C \quad i_U \quad i_V \quad i_W]^T$ is a vector of stator currents,

$\boldsymbol{\varphi_s} = [\varphi_A \quad \varphi_B \quad \varphi_C \quad \varphi_U \quad \varphi_V \quad \varphi_W]^T$ is a vector of stator flux linkages,

$\boldsymbol{\lambda} = [cos\theta_e \quad \cos(\theta_e - \frac{2\pi}{3}) \quad \cos(\theta_e - \frac{4\pi}{3})$

$\cos\left(\theta_e - \frac{\pi}{3}\right) \quad \cos(\theta_e - \pi) \quad \cos(\theta_e - \frac{5\pi}{3})]^T$ is a flux coefficient matrix,

θ_e is the electrical rotor position in radians,

R is stator resistance,

φ_m is permanent magnet flux.

$\boldsymbol{L_s}$ is the inductance coefficient matrix which can be presented as

$$\boldsymbol{L_s} = L_z\boldsymbol{I} + (\tfrac{L_d+L_q-2L_z}{3})\boldsymbol{M_o} + (\tfrac{L_d-L_q}{3})\boldsymbol{M_x} \tag{3}$$

where L_z is the stator leakage inductance, L_d and L_q are stator inductances in d-axis and q-axis respectively. $\boldsymbol{I}$ is a unity matrix with six columns and six rows. $\boldsymbol{M_o}$ and $\boldsymbol{M_x}$ are detailed in Appendix II. The system parameters used in this study are given in Appendix I.

The electromagnetic torque of the PMSM is obtained by taking the partial derivative of the system co-energy with respect to the rotor position angle,

$$T_e = P_P \frac{\partial}{\partial\theta_e}\left(\frac{1}{2}\boldsymbol{i_s}^T\boldsymbol{L_s}\boldsymbol{i_s} + \boldsymbol{i_s}^T\boldsymbol{\lambda}\varphi_m\right) \tag{4}$$

where P_P is the number of pole pairs.

B. Model Representation in dq Rotating Frame

By ignoring zero sequence component, DTP-PMSM can be represented as two single three-phase machines with mutual coupling through transformation matrix T_s.

$$[f_{d1} \quad f_{q1} \quad f_{d2} \quad f_{q2}]^T = T_r[f_A \quad f_B \quad f_C \quad f_U \quad f_V \quad f_W]^T \tag{5}$$

where f stands for variable such as voltage, current or flux.

$$T_r = \begin{bmatrix} T_{r1} & 0 \\ 0 & T_{r2} \end{bmatrix} \tag{6}$$

$$T_{r1} = \frac{2}{3}\begin{bmatrix} cos\theta_e & cos\left(\theta_e - \frac{2\pi}{3}\right) & cos\left(\theta_e + \frac{2\pi}{3}\right) \\ -sin\theta_e & -sin\left(\theta_e - \frac{2\pi}{3}\right) & -sin\left(\theta_e + \frac{2\pi}{3}\right) \end{bmatrix} \tag{7}$$

$$T_{r2} = \frac{2}{3}\begin{bmatrix} cos\left(\theta_e - \frac{\pi}{3}\right) & cos(\theta_e - \pi) & cos\left(\theta_e + \frac{\pi}{3}\right) \\ -sin\left(\theta_e - \frac{\pi}{3}\right) & -sin(\theta_e - \pi) & -sin\left(\theta_e + \frac{\pi}{3}\right) \end{bmatrix} \tag{8}$$

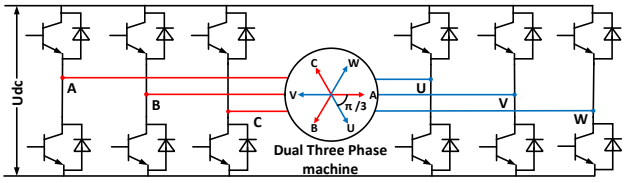

Fig. 1 DTP-PMSM drive system.

C. Model Representation in αβ Stationary Frame

The transformation of variable between dq rotating frame and $\alpha\beta$ stationary frame can be presented as:

$$[f_{\alpha1} \quad f_{\beta1} \quad f_{\alpha2} \quad f_{\beta2}]^T = T_s[f_{d1} \quad f_{q1} \quad f_{d2} \quad f_{q2}]^T \tag{9}$$

$$T_s = \begin{bmatrix} T_{s1} & 0 \\ 0 & T_{s2} \end{bmatrix} \tag{10}$$

$$T_{s1} = T_{s2} = \begin{bmatrix} cos\theta_e & -sin\theta_e \\ sin\theta_e & cos\theta_e \end{bmatrix} \tag{11}$$

III. Back EMF Based Sensorless Control

A. Estimation of Back EMF

The voltage equation in dq rotating frame can be derived from (1)-(2) and (5)-(8)[11]:

$$\begin{bmatrix} u_{d1} \\ u_{q1} \\ u_{d2} \\ u_{q2} \end{bmatrix} = M_1\begin{bmatrix} i_{d1} \\ i_{q1} \\ i_{d2} \\ i_{q2} \end{bmatrix} + \begin{bmatrix} 0 \\ e \\ 0 \\ e \end{bmatrix} \tag{12}$$

where

$$M_1 = \begin{bmatrix} R + s\cdot L_d & -\omega_e L_q & s\cdot L_{dd} & -\omega_e L_{qq} \\ \omega_e L_q & R + s\cdot L_d & \omega_e L_{qq} & s\cdot L_{dd} \\ s\cdot L_{dd} & -\omega_e L_{qq} & R + s\cdot L_d & -\omega_e L_q \\ \omega_e L_{qq} & s\cdot L_{dd} & \omega_e L_q & R + s\cdot L_d \end{bmatrix}$$

e is defined as the extend EMF which presented as:

$$e = (L_d - L_q)(\omega_e(i_{d1} + i_{d2}) - (\dot{i}_{q1} + \dot{i}_{q2})) + \omega_e\varphi_m \tag{13}$$

Since the two sets of three-phase windings are exactly symmetric, if the current controllers of these two dq frames share same parameters, (12) can be expressed as:

$$\begin{bmatrix} u_{d1} \\ u_{q1} \\ u_{d2} \\ u_{q2} \end{bmatrix} = M_2\begin{bmatrix} i_{d1} \\ i_{q1} \\ i_{d2} \\ i_{q2} \end{bmatrix} + \begin{bmatrix} 0 \\ e \\ 0 \\ e \end{bmatrix} \tag{14}$$

where

$$M_2 = \begin{bmatrix} R + s \cdot L_D & -\omega_e L_Q & 0 & 0 \\ \omega_e L_Q & R + s \cdot L_D & 0 & 0 \\ 0 & 0 & R + s \cdot L_D & -\omega_e L_Q \\ 0 & 0 & \omega_e L_Q & R + s \cdot L_D \end{bmatrix}$$

$$L_D = L_d + L_{dd}, L_Q = L_q + L_{qq} \quad (15)$$

Voltage equation in $\alpha\beta$ stationary frame can be deduced combining (9)-(11) and (14)-(15):

$$\begin{bmatrix} u_{\alpha 1} \\ u_{\beta 1} \\ u_{\alpha 2} \\ u_{\beta 2} \end{bmatrix} = M_3 \begin{bmatrix} i_{\alpha 1} \\ i_{\beta 1} \\ i_{\alpha 2} \\ i_{\beta 2} \end{bmatrix} + e \begin{bmatrix} -sin\theta_e \\ cos\theta_e \\ -sin\theta_e \\ cos\theta_e \end{bmatrix} \quad (16)$$

where M_3 is detailed in Appendix II.

According to (16), two sets of three-phase windings can be completely decoupled and voltage equation of DTP-PMSM in $\alpha\beta$ stationary frame can be simplified as

$$u_{\alpha\beta_{1,2}} = Ri_{\alpha\beta_{1,2}} + s \cdot L_D i_{\alpha\beta_{1,2}} + j\omega_e(L_D - L_Q)i_{\alpha\beta_{1,2}} + e_{\alpha\beta_{1,2}} \quad (17)$$

According to [12], a PI type Back EMF estimator consists of two parts: the DTP-PMSM model (17) without the extended EMF ($e_{\alpha\beta_{1,2}}$) and a proportional–integral (PI) compensator. Since the extended EMF is unmodeled, it is inherently estimated by the PI compensator. The schematic diagram of this estimation is shown in Fig. 2. The voltage equation in Fig. 2 can be written as:

$$u_{\alpha\beta_{1,2}} = R\hat{i}_{\alpha\beta_{1,2}} + s \cdot L_D \hat{i}_{\alpha\beta_{1,2}} + j\omega_e(L_D - L_Q)i_{\alpha\beta_{1,2}} + \hat{e}_{\alpha\beta_{1,2}} \quad (18)$$

Combining (17) and (18) gives:

$$(e_{\alpha\beta_{1,2}} - \hat{e}_{\alpha\beta_{1,2}}) + (R + s \cdot L_D)(i_{\alpha\beta_{1,2}} - \hat{i}_{\alpha\beta_{1,2}}) = 0 \quad (19)$$

Since the estimated Back EMF is the output of the PI controller, the following equation exists:

$$-\hat{e}_{\alpha\beta_{1,2}} = (i_{\alpha\beta_{1,2}} - \hat{i}_{\alpha\beta_{1,2}})\left(k_p + \frac{k_i}{s}\right) \quad (20)$$

$$k_p = L_D\omega_{est}, k_i = R\omega_{est} \quad (21)$$

Combining (19)-(21), the following relationship between actual extend EMF and estimated EMF can be given as:

$$\hat{e}_{\alpha\beta_{1,2}} = \frac{\omega_{est}}{s+\omega_{est}} e_{\alpha\beta_{1,2}} \quad (22)$$

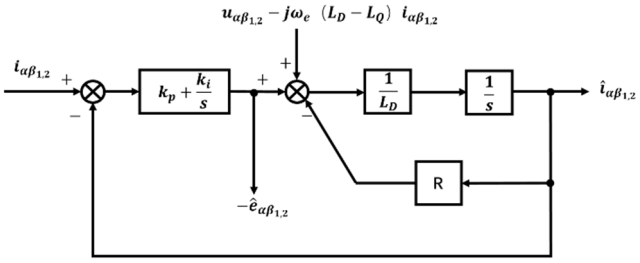

Fig. 2 Back EMF estimator.

B. Estimation of Speed and Position

In this section, two different types of speed and position estimator will be introduced, i.e. PLL type and Luenberger observer type.

1) PLL Type Speed and Position Estimator

The PLL type speed and position estimator is shown in Fig. 3.

From (16), it can be deduced that

$$e_\alpha = e(-sin\theta_e), e_\beta = e(cos\theta_e) \quad (23)$$

According to (23) and (24), the error signal Δe in Fig. 3 can be presented as:

$$\Delta e = -\hat{e}_\alpha cos\hat{\theta}_e - \hat{e}_\beta sin\hat{\theta}_e = k(sin\theta_e cos\hat{\theta}_e - cos\theta_e sin\hat{\theta}_e) = ksin(\theta_e - \hat{\theta}_e) \quad (24)$$

where

$$k = (L_d - L_q)(\hat{\omega}_e(i_{d1} + i_{d2}) - (\dot{i}_{q1} + \dot{i}_{q2})) + \hat{\omega}_e\varphi_m \quad (25)$$

The following approximation exists if $\theta_e - \hat{\theta}_e$ is small enough[12]:

$$\Delta e \approx k(\theta_e - \hat{\theta}_e) \quad (26)$$

Thus, a PI controller can be utilized to correct the position error Δe and make the estimated position converge to the reference one.

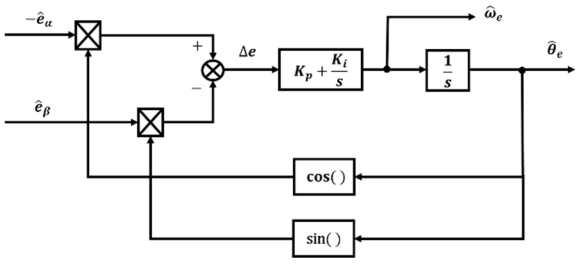

Fig. 3 Block diagram of PLL based speed and position estimator.

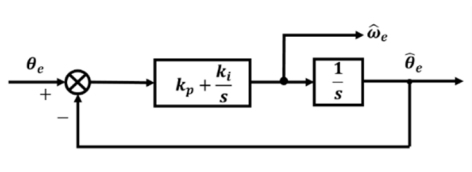

Fig. 4 Equivalent block diagram of PLL based speed and position estimator.

According to (26), Fig. 3 can be simplified equivalently to Fig. 4. The transfer function from θ_e to $\hat{\theta}_e$ in Fig. 4 can be given by:

$$\frac{\hat{\theta}_e}{\theta_e} = \frac{K_p s + K_i}{s^2 + K_p s + K_i} \tag{27}$$

The characteristic equation of the standard second-order system can be written as:

$$\frac{2\xi\omega_n s + \omega_n^2}{s^2 + 2\xi\omega_n s + \omega_n^2} \tag{28}$$

where ξ is damping ratio and ω_n is natural frequency.

By assuming that the denominator of (27) is the same as that of (28), K_p and K_i can be deduced as follows:

$$K_p = 2\xi\omega_n, K_i = \omega_n^2 \tag{29}$$

The transient response of the PLL type estimator can be improved by adding a double integral term into the PI controller as follows:

$$K_1 + \frac{K_2}{s} + \frac{K_3}{s^2} \tag{30}$$

The transfer function from θ_e to $\hat{\theta}_e$ is given by:

$$\frac{\hat{\theta}_e}{\theta_e} = \frac{K_1 s^2 + K_2 s + K_3}{s^3 + K_1 s^2 + K_2 s + K_3} \tag{31}$$

The three gains in (31) are determined to satisfy the following condition:

$$s^3 + K_1 s^2 + K_2 s + K_3 = (s + \omega_n)(s^2 + 2\xi\omega_n s + \omega_n^2) \tag{32}$$

where ξ and ω_n are the same values as in the foregoing simulations.

2) Luenberger Observer Type Speed and Position Estimator

A Luenberger observer type speed and position estimator can also be used for the estimation of rotor speed and position [13] as shown in Fig. 6. The transfer function of the Luenberger observer type position estimator, shown in Fig. 6 is given by (37) [14]

$$\frac{\hat{\theta}_e}{\theta_e} = \frac{JK_a s^2 + (BK_a + K_b)s + K_c}{Js^3 + (JK_a + B)s^2 + (BK_a + K_b)s + K_c} \tag{33}$$

where J is rotational inertia, B is viscous friction.

The gains of the estimator in Fig. 6 can be selected such that the characteristic equation of (33) has the same roots as the followings [14]:

$$K_a = -\alpha, K_b = J\alpha^2, K_c = -J\alpha^3 \tag{34}$$

where α is the root of the characteristic equation.

Fig. 5 shows the bode plots of (30) and (33) where ξ and ω_n are set to 0.5 and 100 rad/s, respectively. As shown in Fig. 5, when the double integral term is added, the phase delay declines and the performance of transient state is improved. Hence, a double integral pulsed PI controller is utilized as PLL estimator.

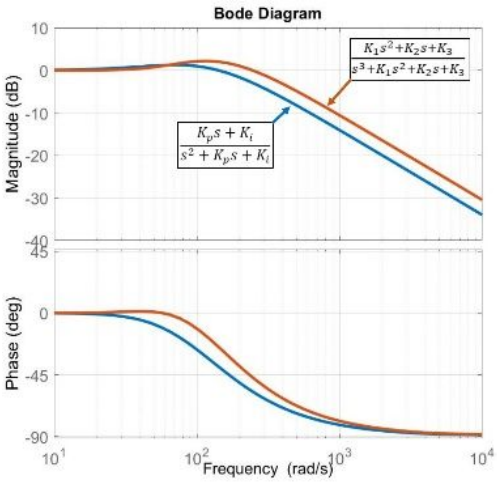

Fig. 5 Bode diagram of PLL type estimators.

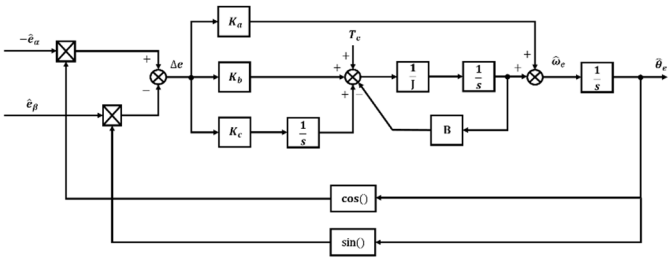

Fig. 6 Block diagram of Luenberger observer based speed and position estimator.

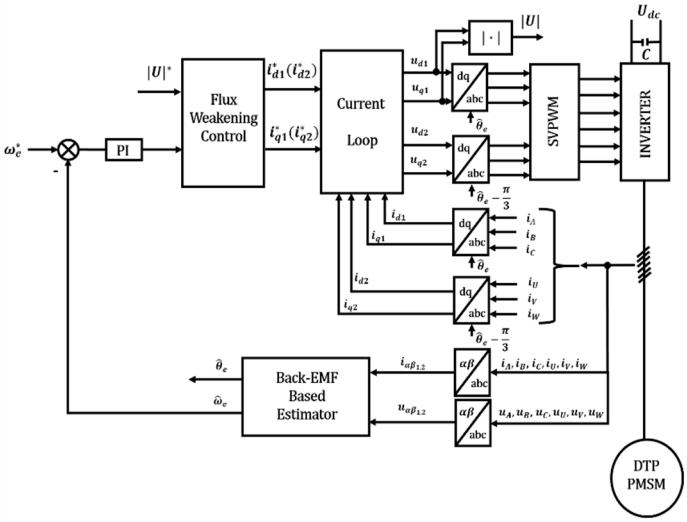

Fig. 7 Block diagram of sensorless control system based on DTP-PMSM

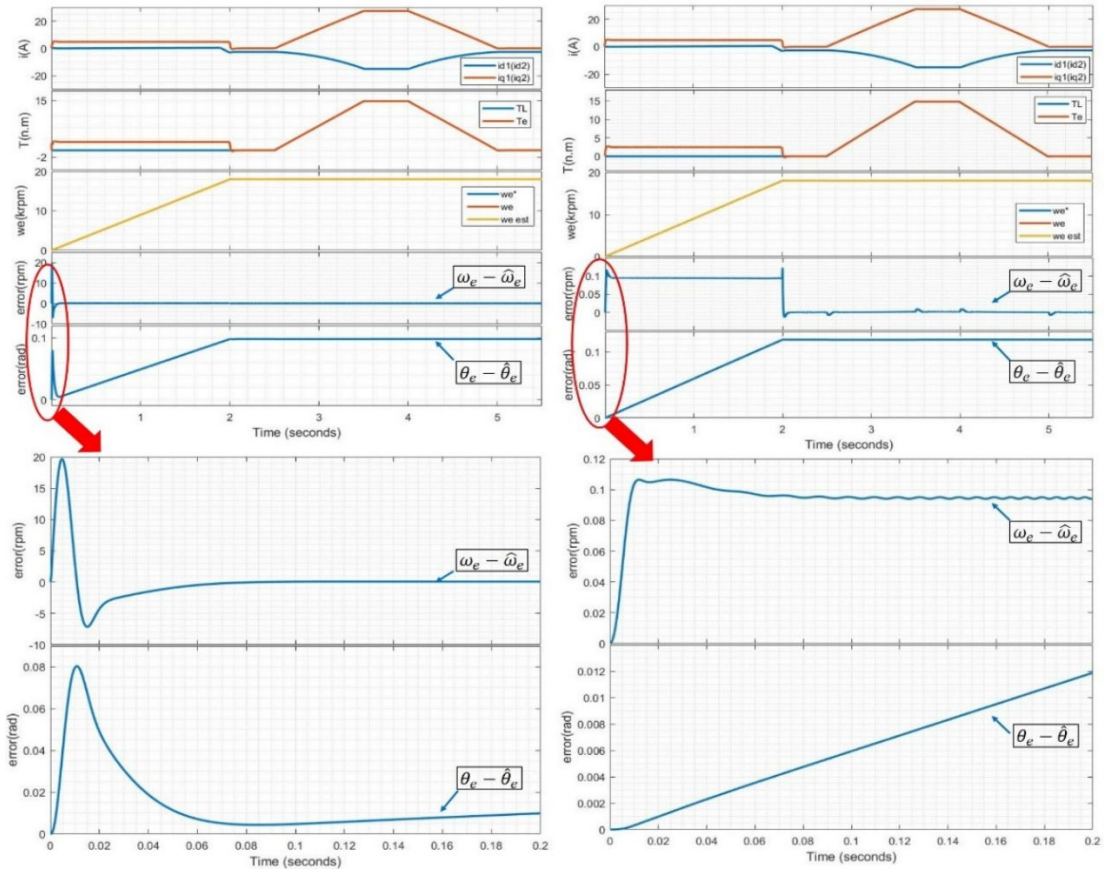

(a) (b)

Fig. 8 Comparison of simulation results (a) PLL type estimator (b) Luenberger observer type estimator

IV. Simulation Results

The block diagram of the sensorless control system is shown in Fig. 7. Simulation results of PLL based back EMF method and Luenberger observer based back EMF method are shown in Fig. 8. The comparison of these two methods is made on the same scenario which can be divided into two stages. The first stage continues from beginning to 2.5 s while the second stage lasts from 2.5 s to the end. In the first stage, there is no load torque and rotor speed increases steadily from 0 rpm to 18 krpm during the first two seconds and retains at 18 krpm afterwards. In the second stage, a torque load is applied. The torque load grows steadily from 0 $\mathrm{N \cdot m}$ to 100% load (14.8 $\mathrm{N \cdot m}$) between 2.5 s and 3.5 s and then stays at 14.8 $\mathrm{N \cdot m}$ for 1 s. After unloading from 100% load to 0 $\mathrm{N \cdot m}$ between 4 s and 5 s, it keeps at 0 $\mathrm{N \cdot m}$ to the end of simulation.

The aims of using sensorless control in this study is achieved according to Fig. 8. Satisfactory performance of current is observed and flux weakening control is thereby verified after calculation. System keeps at stable status as variable load torque is applied. The tracking of speed reference (ω_e^*) is satisfactory. Yet, there are some differences of speed and position estimation between control performance obtained using PLL type estimator and Luenberger type estimator. The Luenberger type estimator has a better dynamic performance which can be observed especially in the partial enlargement figure during dwell 0 s to 0.2 s. This advantage is due to include the demanded torque as a feed forward term [15] as shown in Fig. 5. Luenberger observer type estimator is parameter dependent although it provides the best dynamic response [16]. Besides, high frequency noise is observed in the estimated speed obtained using Luenberger observer type estimator. In contrast, the high frequency component in the estimated speed error is filtered by the PLL type estimator since the estimator and the low-pass filter share a same frequency.

Conclusions

Two back EMF based estimators for the sensorless control of a DTP-PMSM are investigated in this study. S-domain simulations are conducted to compare the effectiveness of these two estimators. Luenberger type estimator has better dynamic performance but suffers high frequency noise in the estimated speed error and requires the use of machinal parameters. In contrast, PLL type estimator has inferior but acceptable performance. Its low-pass characteristics frees it from the high frequency noise. Moreover, it does not require the use of mechanical parameters. PLL type estimator is preferred in further study and potential applications due to its simpler structure and independence from mechanical parameters.

Acknowledgment

This project has received funding from the Clean Sky 2 Joint Undertaking under the European Union's Horizon 2020 research and innovation program under grant agreement No 737814.

REFERENCE

[1] Levi, E., *Multiphase electric machines for variable-speed applications.* IEEE Transactions on industrial electronics, 2008. **55**(5): p. 1893-1909.

[2] Karttunen, J., et al. *Dual three-phase permanent magnet synchronous machine supplied by two independent voltage source inverters*. in *Power Electronics, Electrical Drives, Automation and Motion (SPEEDAM), 2012 International Symposium on*. 2012. IEEE.

[3] Singh, G.K., K. Nam, and S. Lim, *A simple indirect field-oriented control scheme for multiphase induction machine.* IEEE Transactions on Industrial Electronics, 2005. **52**(4): p. 1177-1184.

[4] Bojoi, R., et al., *Vector control of dual-three-phase induction-motor drives using two current sensors.* IEEE Transactions on Industry Applications, 2006. **42**(5): p. 1284-1292.

[5] Bojoi, R., et al., *Digital field-oriented control for dual three-phase induction motor drives.* IEEE Transactions on Industry Applications, 2003. **39**(3): p. 752-760.

[6]. Scelba, G., et al. *Compensation of rotor positon estimation errors in sensorless dual-three phase PMSM drives through back-EMF sensing*. in *Sensorless Control for Electrical Drives (SLED), 2017 IEEE International Symposium on*. 2017. IEEE.

[7] Bojoi, R., et al. *Multiphase PM machine for more electric aircraft applications: Prototype for design validation*. in *IECON 2012-38th Annual Conference on IEEE Industrial Electronics Society*. 2012. IEEE.

[8] Xu, P. and Z. Zhu, *Initial rotor position estimation using zero-sequence carrier voltage for permanent-magnet synchronous machines.* IEEE Transactions on Industrial Electronics, 2017. **64**(1): p. 149-158.

[9] Raca, D., et al., *Carrier-signal selection for sensorless control of PM synchronous machines at zero and very low speeds.* IEEE Transactions on Industry Applications, 2010. **46**(1): p. 167-178.

[10] Consoli, A., G. Scarcella, and A. Testa, *Industry application of zero-speed sensorless control techniques for PM synchronous motors.* IEEE Transactions on Industry Applications, 2001. **37**(2): p. 513-521.

[11] Morimoto, S., et al. *Sensorless control strategy for salient-pole PMSM based on extended EMF in rotating reference frame*. in *Industry Applications Conference, 2001. Thirty-Sixth IAS Annual Meeting. Conference Record of the 2001 IEEE*. 2001. IEEE.

[12] Dienes, P., *The Taylor series: an introduction to the theory of functions of a complex variable*. 1957: Dover New York, NY.

[13] Kim, H., M.C. Harke, and R.D. Lorenz, *Sensorless control of interior permanent-magnet machine drives with zero-phase lag position estimation.* IEEE Transactions on Industry Applications, 2003. **39**(6): p. 1726-1733.

[14] Sul, S.-K., *Control of electric machine drive systems*. Vol. 88. 2011: John Wiley & Sons.

[15] Jiang, H., *Audible noise reduction in the high frequency injection based sensorless torque control for EPS applications*. 2012, University of Nottingham.

[16] Duan, Y., *A comparison of saliency based sensorless control techniques for a PM machine*. 2012, University of Nottingham.

Appendix I

Table 1 Parameters of machine.

Parameter	***Mark***	***Value***	***Unit***
Phase Resistance	R	0.41	Ohm
D-axis Inductance	L_d	365	μH
Q-axis Inductance	L_q	410	μH
Rotational Inertia	J	0.00263	kg·m^2
Peak No-load Flux Linkage per Channel	φ_m	0.0287	V·s
Pole Pairs Number	P_P	6	/

Appendix II

$\boldsymbol{M_o}$ and $\boldsymbol{M_x}$ are matrixes in (3). M_3 is matrix in (16).

$$\boldsymbol{M_o} = \begin{bmatrix} 1 & -\frac{1}{2} & -\frac{1}{2} & \frac{1}{2} & -1 & \frac{1}{2} \\ -\frac{1}{2} & 1 & -\frac{1}{2} & \frac{1}{2} & \frac{1}{2} & -1 \\ -\frac{1}{2} & -\frac{1}{2} & 1 & -1 & \frac{1}{2} & \frac{1}{2} \\ \frac{1}{2} & \frac{1}{2} & -1 & 1 & -\frac{1}{2} & -\frac{1}{2} \\ -1 & \frac{1}{2} & \frac{1}{2} & -\frac{1}{2} & 1 & -\frac{1}{2} \\ \frac{1}{2} & -1 & \frac{1}{2} & -\frac{1}{2} & -\frac{1}{2} & 1 \end{bmatrix}$$

.

$$\boldsymbol{M_x} = \begin{bmatrix} cos2\theta & cos\left(2\theta-\frac{2\pi}{3}\right) & cos\left(2\theta+\frac{2\pi}{3}\right) & cos\left(2\theta-\frac{\pi}{3}\right) & cos(2\theta-\pi) & cos\left(2\theta+\frac{\pi}{3}\right) \\ cos\left(2\theta-\frac{2\pi}{3}\right) & cos\left(2\theta+\frac{2\pi}{3}\right) & cos2\theta & cos(2\theta-\pi) & cos\left(2\theta+\frac{\pi}{3}\right) & cos\left(2\theta-\frac{\pi}{3}\right) \\ cos\left(2\theta+\frac{2\pi}{3}\right) & cos2\theta & cos\left(2\theta-\frac{2\pi}{3}\right) & cos\left(2\theta+\frac{\pi}{3}\right) & cos\left(2\theta-\frac{\pi}{3}\right) & cos(2\theta-\pi) \\ cos\left(2\theta-\frac{\pi}{3}\right) & cos(2\theta-\pi) & cos\left(2\theta+\frac{\pi}{3}\right) & cos\left(2\theta-\frac{2\pi}{3}\right) & cos\left(2\theta-\frac{4\pi}{3}\right) & cos2\theta \\ cos(2\theta-\pi) & cos\left(2\theta+\frac{\pi}{3}\right) & cos\left(2\theta-\frac{\pi}{3}\right) & cos\left(2\theta-\frac{4\pi}{3}\right) & cos2\theta & cos\left(2\theta-\frac{2\pi}{3}\right) \\ cos\left(2\theta+\frac{\pi}{3}\right) & cos\left(2\theta-\frac{\pi}{3}\right) & cos(2\theta-\pi) & cos2\theta & cos\left(2\theta-\frac{2\pi}{3}\right) & cos\left(2\theta-\frac{4\pi}{3}\right) \end{bmatrix}$$

$$M_3 = \begin{bmatrix} R+s\cdot L_D & \omega_e(L_D-L_Q) & 0 & 0 \\ -\omega_e(L_D-L_Q) & R+s\cdot L_D & 0 & 0 \\ 0 & 0 & R+s\cdot L_D & \omega_e(L_D-L_Q) \\ 0 & 0 & -\omega_e(L_D-L_Q) & R+s\cdot L_D \end{bmatrix}$$